Theory of Auger core-valence-valence processes in simple metals. II. Dynamical and surface effects on Auger line shapes

C.-O. Almbladh and A. L. Morales*
Department of Theoretical Physics, Lund University, Sölvegatan 14A, S-223 62 Lund, Sweden
(Received 11 April 1988)

Auger *CVV* spectra of simple metals are generally believed to be well described by one-electron-like theories in the bulk which account for matrix elements and, in some cases, also static core-hole screening effects. We present here detailed calculations on Li, Be, Na, Mg, and Al using self-consistent bulk wave functions and proper matrix elements. The resulting spectra differ markedly from experiment and peak at too low energies. To explain this discrepancy we investigate effects of the surface and dynamical effects of the sudden disappearance of the core hole in the final state. To study core-hole effects we solve Mahan–Nozières–De Dominicis (MND) model numerically over the entire band. The core-hole potential and other parameters in the MND model are determined by self-consistent calculations of the core-hole impurity. The results are compared with simpler approximations based on the final-state rule due to von Barth and Grossmann. To study surface and mean-free-path effects we perform slab calculations for Al but use a simpler infinite-barrier model in the remaining cases. The model reproduces the slab spectra for Al with very good accuracy. In all cases investigated either the effects of the surface or the effects of the core hole give important modifications and a much improved agreement with experiment.

I. INTRODUCTION

To calculate Auger core-valence-valence (*CVV*) line shapes in solids is quite a demanding problem even within a one-electron picture. The first realistic one-electron calculation was presented about ten years ago by Feibelman *et al.*,[1] who considered the $L_{2,3}VV$ spectrum from a silicon surface. The work of Feibelman *et al.* demonstrated the importance of matrix-element effects, which tend to select *sp* and *pp* contributions, and showed the simpler pictures based on self-folded densities of states to be inadequate. Later Jennison and co-workers[2–4] presented a large number of calculations based on realistic wave functions and obtained a good overall agreement with experiment. A major conclusion of Jennison and co-workers is that neither surface nor dynamical core-hole effects need to be invoked in order to explain Auger *CVV* line shapes. However, the mean free path of the Auger electron is of the order of only a few atomic distances at typical Auger energies of about 100 eV, and thus one would expect effects of the surface. In addition, model calculations by Schulman and Dow[5] for lithium suggest that dynamical effects may be quite important.

In this work we will reconsider the problem of calculating Auger line shapes of solids from first principles, and as in the preceding paper,[6] henceforth to be referred to as I, we will confine ourselves to the Li, Be, Na, Mg, and Al metals. We present detailed one-electron spectra from a bulk atom calculated from self-consistent linear muffin-tin-orbital (LMTO) wave functions[7,8] and find, quite unexpectedly, results which in general do not agree well with experiment. (Here, and in the following, "one-electron results" refers to results which account for the Coulomb matrix elements from ground-state orbitals.) One may perhaps argue that the LMTO method is not accurate enough for obtaining good one-electron spectra. However, the overall experience over the past ten years is that the LMTO method for calculating electronic structure is capable of giving numerically accurate values for structural energies, charge densities, cohesive energies, etc.[8,9] In the present case we are dealing with close-packed or almost-close-packed systems, for which the LMTO method is particularly well suited. We would also like to remind the reader that in previous work by von Barth and Grossmann[10,11] the LMTO method has proven to yield an accurate description of both main x-ray-emission bands as well as core-hole effects in x-ray satellite and Auger *KLV* spectra. Thus we believe our results to be genuine and not artifacts of the numerical procedure used for solving orbital Schrödinger equations.

In general, our one-electron bulk calculations give spectra which peak at lower Auger-electron energies than do the corresponding experimental results. The discrepancy can easily be removed by adjusting the different partial wave contributions (*ss*,*sp*,*pp*), but in order to justify such procedures one must go beyond strict one-electron theory. To resolve the reason for the discrepancies we will study screening and dynamical effects from the core hole present in the initial state of the Auger process, and effects of the surface and mean free path. As we will show, both effects can lead to a peak shift to higher energies and give, when combined, results in much better agreement with experiment. Interestingly enough, however, in each individual case studied here *either* the surface effects are important *or* the core-hole effects. Thus, the explanation is different in each case.

The simplest model that accounts for core-hole effects in a dynamical way is the independent fermion model of Mahan, Nozières, and De Dominicis (MND).[12] In this model, one represents the system with an effective one-

electron Hamiltonian H^* in the initial core-hole state, and a different one-electron Hamiltonian H in the final state without a core hole. To model H and H^* we perform self-consistent supercell calculations, as described in I, on systems where every 16th atom is a core-hole atom, in addition to the ground-state calculations. We choose H and H^* such that they produce one-electron spectra which agree with our LMTO results without and with a static core-hole, respectively. In this fitting procedure we decompose the Auger spectrum into subchannels according to the angular momenta and spin of the two valence holes left behind, and do the fit in each subchannel separately. To obtain a fully dynamical spectrum we then solve the model numerically using the finite-N method pioneered by Kotani and Toyozawa.[13] In a number of previous works,[10,14,15] this method has proven to rather easily give reliable numerical results. Including p waves, our present calculation involves eight subchannels.

As shown by von Barth and Grossmann,[10] the *shape* of a dynamical (subchannel) spectrum generally agrees well with the one-electron spectrum obtained from orbitals solved in the *final-state* potential. This result was termed the final-state rule. In the case of emission the final-state potential contains no core hole. The total and partial yields, on the other hand, are determined by the valence-electron wave function in the initial core-hole state (see I and references therein). In this work we will also study approximations used by Ramaker[16] and Jennison[3] which are based on the final-state rule and yield sum rules.

To estimate the surface and mean-free-path effects we perform self-consistent slab calculations in the case of Al. We use these slab results to justify a simpler surface model which we use for the remaining systems. In the simplified model we extend an idea by Gadzuk[17] and represent a valence orbital near the surface by a Bloch wave specularly reflected in a surface plane about one atomic radius outside the outermost nuclei. This corresponds to an infinite-barrier model (IBM) where the secondary reflected rays have been neglected. The IBM is clearly a somewhat crude model for the surface-electronic structure, but, owing to the broad selection rules imposed by Auger matrix elements, we do not expect an Auger spectrum to probe the finer details in the local electronic structure near the surface.

By and large the present work relies heavily on effective one-electron models. The one-electron picture has proven to be quite successful for interpreting photoemission and other spectra which mainly involve one-hole final states. In Auger emission, on the other hand, the final states involve *two* valence holes initially localized on the same atomic site, and as a consequence of hole-hole interactions one might expect important deviations from an independent fermion description even for a simple metal. As is well known, such interactions play an important role in narrow d bands,[18] but our results do not indicate this to be the case for s- and p-like bands. A second aspect neglected in the effective one-electron models used here is the coupling between the primary core-hole creation process and the subsequent Auger emission. However, as we have shown in the preceding paper, the core-hole lifetimes encountered here are long enough for the shakeup cloud of plasmons and particle-hole pairs created in the primary step to diffuse away completely before the reemission event, leaving a completely relaxed core hole behind.[19,20] Thus we can with confidence take the initial state of the Auger process as the fully relaxed hole state. A more important aspect left out in our work is the effect of collective excitations, i.e., the plasmon satellites. These satellites are both of intrinsic and extrinsic origin[21] and are often quite strong. To fully account for these effects a dynamical theory of interacting rather than noninteracting valence electrons is required. Although the principles for such a theory are more or less known, a realistic quantitative description of plasmon satellites in Auger spectra has yet to come. In the absence of such a description experimentalists usually deconvolute away the plasmon-loss effects, assuming that they enter in the same way as in x-ray photoemission spectra, in order to obtain an underlying "one-electron" spectrum. Although such a procedure is quite useful in many respects and the best one can do at present, it must be remembered that those parts of an experimental deconvoluted spectrum which overlap with strong loss satellites must be regarded with some skepticism.

II. THE NO-LOSS AUGER CURRENT FROM A SURFACE

A. General

The one-electron expressions used for the bulk spectra are given in I and need not be repeated. To obtain the no-loss Auger current coming through the surface we should, according to general photoemission theory,[22] take the final Auger orbital ϕ_A as a time-reversed LEED (low-energy electron diffraction) orbital solved in the potential

$$V_{\text{eff}} = V_C + \Sigma_{\tilde{c}}(\varepsilon_A) \tag{1}$$

inside the solid. In Eq. (1) V_C is the total Coulomb potential and $\Sigma_{\tilde{c}}(\varepsilon_A)$ the (time-reversed) one-electron self-energy or optical potential at the Auger energy ε_A. In what follows we make the usual approximation and replace Σ by $v_{\text{xc}} + i\gamma/2$, where v_{xc} is the Hohenberg-Kohn-Sham[23] ground-state potential and where the constant damping γ is taken from electron-gas calculations or deduced from experimental mean free paths. Referring specifically to one-electron theory, we can write the angle-resolved Auger current in direction $\hat{\mathbf{n}}$ from a specific site j as

$$D_j(\varepsilon_A,\hat{\mathbf{n}}) = 2\pi \sum_{k,l}^{\text{occ}} \left(|\langle kl|v|c\phi_A\rangle|^2 - \langle kl|v|\phi_A c\rangle^* \langle kl|v|c\phi_A\rangle \right) D_0(\varepsilon_A)\delta(\varepsilon_k + \varepsilon_l - \varepsilon_A - \varepsilon_c) , \tag{2}$$

where $D_0(\varepsilon) = (2\varepsilon)^{1/2}/8\pi^3$ is the state density per spin in vacuum. (Regarding notations and units, see I.) Before proceeding we note that the time-reversed LEED states enter because we here count only a subclass of final states corre-

sponding to no-energy losses and a given emission angle, and that they are thus not to be used for calculating lifetimes which involve all possible decay events.

In the present calculation we adopt the simplest possible approximation for ϕ_A and take it as a plane wave of the appropriate direction in vacuum, and a properly damped linear augmented plane wave (LAPW) inside the solid with the behavior

$$\phi_A(\mathbf{r})=\exp[i\mathbf{k}_A\cdot\mathbf{R}_j-(\lambda Z_j/\cos\theta)]\sum_{L_A} i^l\phi_{L_A}(\varepsilon_A,\hat{\mathbf{n}},|\mathbf{r}-\mathbf{R}_j|)Y_{L_A}((\mathbf{r}-\mathbf{R}_j)/|\mathbf{r}-\mathbf{R}_j|) \tag{3}$$

inside the muffin tin or atomic sphere at site j. [As in paper I, we shall use the atomic-sphere approximation (ASA).] In Eq. (3) $2\lambda=\gamma/k_A$ is the inverse mean free path, L_A is short for the Auger-electron angular momentum labels, and θ is the emission angle. We have chosen our coordinate system so as to have the surface along the plane $z=0$. To proceed we approximate the valence orbitals by muffin-tin or ASA orbitals,

$$\phi_k(\mathbf{r})=\exp(i\mathbf{k}_\parallel\cdot\mathbf{R}_j)\sum_L i^l C_{jL}^k Y_L((\mathbf{r}-\mathbf{R}_j)/|\mathbf{r}-\mathbf{R}_j|)\phi_{jl}(\varepsilon,|\mathbf{r}-\mathbf{R}_j|) \tag{4}$$

($\mathbf{k}_\parallel$ is the momentum parallel to the surface), do a multipole expansion of the Coulomb matrix elements as in I, keep only the central cell part, and form the Auger intensity according to Eq. (2). In the presence of a surface the sum over magnetic sublabels (m) can no longer be performed analytically. Averaging over the core-hole magnetic and spin sublevels and summing the contribution from all atomic layers we obtain an expression of the form

$$\begin{aligned}D(\varepsilon_A,\hat{\mathbf{n}})=2\pi\sum_j e^{-2\lambda Z_j/\cos\theta}\int_{-\infty}^{\mu}d\varepsilon\int_{-\infty}^{\mu}d\varepsilon' D_0(\varepsilon_A)\delta(\varepsilon+\varepsilon'-\varepsilon_c-\varepsilon_A)\\ \times\frac{1}{2l_c+1}\sum_{m_c}\sum_{L_1,L_1'}\sum_{L_2,L_2'}F_{jL_1'L_1}(\varepsilon)F_{jL_2'L_2}(\varepsilon')\\ \times[2Q_j^*(L_c,L_1',L_2',\varepsilon,\varepsilon')\\ -Q_j^*(L_c,L_2',L_1',\varepsilon',\varepsilon)]Q_j(L_c,L_1,L_2,\varepsilon,\varepsilon')\ ,\end{aligned} \tag{5}$$

where

$$F_{jLL'}(\varepsilon)=\sum_k i^{l-l'}C_{jL}^k(C_{jL'}^k)^*\delta(\varepsilon-\varepsilon_k) \tag{6}$$

is a (nondiagonal) state-density function for one spin in the unit cell at $\mathbf{R}_j$, and where

$$Q_j(L_c,L',L,\varepsilon,\varepsilon')=\sum_{k,L_A} i^{l_A}c_k(L,L_c)c_k(L_A,L')R_k(\varepsilon jl,\varepsilon' jl',c,\phi_{L_A}(\varepsilon_A,\hat{\mathbf{n}}))\delta_{m_A+m_c-m-m'} \tag{7}$$

contains the matrix elements. [Here μ is the Fermi level, $c_k(L,L')$ a Gaunt coefficient defined as in Ref. 24, and R_k a Slater integral defined as in I.] Equation (5) can easily be generalized to a more realistic treatment of the final Auger orbital and gives then the general one-electron result for Auger emission from a surface in terms of muffin-tin or ASA wave functions. The results above closely resemble the linear combination of atomic orbitals (LCAO) expressions obtained earlier by Feibelman *et al.*[1]

B. Modeling wave functions near a surface

In the case of Al we model an ideal (100) surface by self-consistent calculations on a repeated slab with 13 Al layers separated by five vacuum layers. We use the LMTO method with wave-function reconstruction as described in I, and calculate the orbitals, which include d waves, for 78 $\mathbf{k}$ points in the irreducible surface wedge.

In the remaining cases we use an infinite-barrier model and represent an orbital (ϕ_k) close to the surface by a Bloch wave (ψ_k) specularly reflected in a surface plane, i.e., we take

$$\phi_k=2^{-1/2}(\psi_k-R\psi_k)\ . \tag{8}$$

Now, with a suitable choice of relative phases of Bloch waves for different k we have $T\psi_k=\psi_{Tk}$ for point-symmetry operations T and for nondegenerate $\mathbf{k}$ points. Using this property it is not difficult to see that the muffin-tin amplitudes B_L^k in

$$\psi_k(\mathbf{r})=\exp(i\mathbf{k}\cdot\mathbf{R}_j)\sum_L i^l B_L^k Y_L((\mathbf{r}-\mathbf{R}_j)/|\mathbf{r}-\mathbf{R}_j|)\phi_l(\varepsilon,|\mathbf{r}-\mathbf{R}_j|)$$

transform as $Y_L^*(\hat{\mathbf{k}})$ under point-symmetry operations.[25] It now readily follows that the approximation in Eq. (8) corresponds to choosing the muffin-tin amplitudes C_{jL}^k in ϕ_k as [cf. Eq. (4)]

$$C_{jL}^k=\frac{e^{ik_zZ_j}}{2^{1/2}}B_L^k[1-(-1)^{m+l}e^{-2ik_zZ_j}]$$

for lattices where the reflection R is an allowed point-group operation. This gives now a state-density function F of the form

$$F_{jLL'}(\varepsilon)=\tfrac{1}{2}\sum_{\mathrm{BZ}}\delta(\varepsilon-\varepsilon_k)i^{l-l'}B_L^k(B_{L'}^k)^*[1-(-1)^{m+l}e^{-2ik_zZ_j}][1-(-1)^{m'+l'}e^{2ik_zZ_j}]\ . \tag{9}$$

The local projected density of states (PDOS) is given by

$$D_{jl}(\varepsilon)=\sum_m F_{jLL}(\varepsilon)\ . \tag{10}$$

In our derivation we considered only nondegenerate **k** points but, since we in Eq. (9) sum over all bands, degenerate as well as nondegenerate, one can show that this restricting assumption is actually not needed.

Far inside the solid, terms which involve the oscillatory terms involving $\exp(\pm i2k_zZ_j)$ give no contribution, and $F_{jLL'}$ properly reduces to its bulk form

$$F_{\infty LL'}(\varepsilon)=\tfrac{1}{2}\sum_{\mathrm{BZ}}\delta(\varepsilon-\varepsilon_k)i^{l-l'}[B_L^k(B_{L'}^k)^*+B_L^{Rk}(B_{L'}^{Rk})^*]=\sum_{\mathrm{BZ}}\delta(\varepsilon-\varepsilon_k)i^{l-l'}B_L^k(B_{L'}^k)^*\ ,$$

which, as discussed in I, reduces to

$$\frac{1}{2l+1}D_l(\varepsilon)\delta_{LL'}$$

for s and p electrons. Closer to the surface the state density begins to deviate from the bulk behavior but, as we will show in Sec. IV, appreciable deviations occur only in the first atomic layer.

In the IBM, Eq. (8), charge neutrality of a surface atom is not guaranteed. Choosing the surface plane one muffin-tin radius outside the outermost nuclei, we obtain for Al a charge depletion of about 0.1 electrons per atom. We think this is not unreasonable and that it can be considered as a crude modeling of the dipole layer, which is formed by a small fraction of electrons being transferred into an exponentially decaying density profile outside the surface. For the monovalent metals this choice of surface plane gives a larger depletion, about 0.3 electrons, which is unacceptably large in comparison with the number of valence electrons. By choosing the plane 1 Wigner-Seitz radius outside the outermost nuclei we obtain a more satisfactory depletion of about 0.1 electrons. The shape of the local projected density of states (PDOS) as well as the shape of the Auger spectrum for an atom at the surface is almost unchanged by this modification, but too much charge depletion makes the Auger current from the first sublayer too small.

In order to evaluate the IBM state-density function $F_{jLL'}(\varepsilon)$, we use LMTO wave functions for the ground state, obtained as described in I, and use a sufficient number of **k** points to converge up to the third sublayer. The fourth and the following sublayers we take as bulk layers. For the cubic metals we use about 1000 **k** points in the irreducible wedge and obtain the contributions from the remaining wedges by the appropriate symmetry transformations. For the hcp metals we use a similar method with about 2000 points in $\frac{1}{12}$ of the first Brillouin zone.

III. DYNAMICAL CORE-HOLE EFFECTS

A. The MND independent fermion model

In the Mahan–Nozières–De Dominicis[12] (MND) model one represents the valence-electron system by different one-electron Hamiltonians in the initial core-hole and in the final no-hole states. We here denote these Hamiltonians by H^* and H, respectively. As is well known, this model can be solved analytically very close to the emission or absorption edge and gives for metals a singular edge behavior which has given rise to much controversy in the past.[26,27] More importantly, the model can be solved also away from the edge by numerical means.[10,13–15,28] Away from threshold the MND model lacks formal justification, but when used with proper parameters (one-electron eigenvalues, core-hole potentials, etc.) obtained from realistic calculations the model has nevertheless been shown to give a good description of x-ray-emission and -absorption bands in most simple metals.[10,11,14] In view of this it is not unreasonable to assume that useful insight can be gained by applying the MND model to the case of Auger CVV emission.

The MND singularity is of the form

$$D(\varepsilon)\sim|\varepsilon-\varepsilon_c|^{-\alpha} \tag{11}$$

close to the edge $\varepsilon=\varepsilon_c$. The exponents α for different kinds of spectra [x-ray photoemission spectroscopy (XPS), x-ray absorption, etc.] can all be expressed in a common set of Fermi-surface phase shifts of the core-hole potential. For the case of Auger CVV emission the exponents are negative (see Ref. 29, Table VI), but in general the leading edge is steeper than it would be in one-electron theory (in the latter case $\alpha=-1$). These effects would move the peak in the spectra to higher energies. On the other hand, the MND model also gives a broadening away from the edge originating from particle-hole shakeup, which tends to move the peak to lower energies. Thus, it is difficult to say anything definite without explicit numerical solutions over the entire spectral range.

The singular-edge behavior was under intense discussion during the 1970s. The picture that has emerged is that the effect is no doubt present and that there is reasonable agreement between theory and experiment in most simple metals (for a recent review, see Ref. 29). In Li, however, there seems to be a conflict between compatibility relations[26] imposed by MND theory and inelastic-electron-scattering experiments.[30] In these experiments the expected enhancement of the s-wave part near the edge was far too small and in fact not possible to

detect. In view of these results it would not be surprising if the MND model overemphasizes the edge enhancement also for the Li Auger spectrum.

As has been shown by Langreth,[31] the MND model can actually be considered as an approximation of a more accurate treatment where the valence-electron interparticle interaction is kept. On the basis of these ideas it has been verified that the interaction between the valence electrons does not alter the edge behavior.[32] In other words, it is still given by Fermi-surface phase shifts which fulfill a generalized Friedel sum rule. Similar results are obtained if band-structure effects are also incorporated in the theory. Thus, the compatibility relations remain valid, and so the problem with the Li data. In all of these generalizations the core hole is considered structureless. In reality it has a spin which can change its direction, and in the case of Li the spin-dependent coupling to the valence electrons has been calculated and shown to be large.[33] Thus, in order to better understand the lithium core spectra, one probably has to solve a dynamic Kondo-like spin problem, and it is not at all clear that asymptotic solutions near the edge are sufficient. The progress made so far is limited, and for further discussions the reader is referred to Ref. 29.

B. The final-state rule

The final-state rule for spectral shapes was originally formulated for x-ray spectra by von Barth and Grossman.[10] They studied MND models with a variety of different potentials and parameters and compared the resulting dynamical spectra with the corresponding one-electron results obtained with and without a core hole. In all cases investigated they found a systematic agreement in shape between the dynamical spectra and the one-electron results obtained with the final-state potential. In the case of emission this potential contains no core hole. von Barth and Grossmann also found a systematic agreement between experimental x-ray-emission spectra and one-electron ground-state results. Spectra calculated with a static core hole, on the other hand, showed strong s resonances which are not seen experimentally. Thus the final-state rule has direct experimental support as well.

As opposed to x-ray spectra, Auger CVV spectra involve many subchannels of comparable intensities. The final-state rule explained above pertains to each subchannel *line shape* $D_{ll'}(\varepsilon)$, but the subchannel yields $\Gamma_{ll'}$ obey an *initial-state rule* and are determined by the valence wave function in the completely relaxed initial state (see I and references therein). This rule is obeyed by the MND model but follows from far more general assumptions. Combining these two results we are led to an approximation for Auger spectra used by Ramaker[16] in which we superimpose subchannel intensities without core-hole effects with weights determined by the initial-state rule for emission yields. Thus,

$$D(\varepsilon_A)=\sum_{\substack{l,l' \\ (l\geq l')}} \frac{\Gamma^*_{ll'}}{\Gamma^o_{ll'}} D^o_{ll'}(\varepsilon_A)\ , \tag{12}$$

where the superscripts o and $*$ refer to one-electron results without and with a static core hole, respectively.

More refined final-state approximations have also been developed in which the final-state one-electron line shapes are augmented with the appropriate MND singularity factors.[10] In this way one obtains a more faithful representation of the dynamical MND results. In this work, however, we want to compare our fully dynamical treatment with an alternative scheme that relies less directly on MND theory, and for this reason we choose the simpler form in Eq. (12).

C. The finite-N method

The simple physical idea behind the finite-N method for solving the MND equations is that local spectral properties of an infinite fermion system can be well simulated by a system containing a finite but large number of fermions. Practical experience as well as comparisons with results by other means have shown that about 100 particles per $lm\sigma$ subchannel is more than sufficient in order to obtain a good representation of the $N\rightarrow\infty$ results.

Now, since the MND model is inherently an independent-electron model, all results can be expressed in Slater determinants. Furthermore, the different channels are assumed not to interact with each other, which allows us to write H and H^* as

$$H=\sum_L H_L,\quad H^*=\sum_L H^*_L\ . \tag{13}$$

[In this section L is short for angular momentum (lm) and spin (σ) labels, and quantities connected with the core-hole Hamiltonian will be denoted by an asterisk ($*$).] Owing to this property the transition amplitudes $\langle s|T|*\rangle$ of a spectral density factorize into matrix elements from each L channel separately (s labels the possible final states). A passive channel L, whose electrons are not involved in the transition operator T, gives a mere overlap $\langle N,s|N^*\rangle_L$ between initial and final states with N electrons, whereas an active channel L' gives matrix elements involving one ($\langle N-1,s|c_{L'k}|N^*\rangle_{L'}$) or two ($\langle N-2,s|c_{L'k}c_{L'k'}|N^*\rangle_{L'}$) electron operators $c_{L'k}$ of the no-hole Hamiltonian $H_{L'}$. As a consequence of this, we obtain the complete spectrum

$$D(\varepsilon)=\sum_s |\langle s|T|*\rangle|^2\,\delta(E_*-E_s-\varepsilon) \tag{14}$$

by convoluting recoil spectra $[A_l(\varepsilon)]$ from the passive channels with one-electron spectra $[B_l(\varepsilon)]$ and possibly two-electron spectra from the active channels.

Consider, e.g., the recoil spectrum

$$A_l(\varepsilon)=\sum_s |\langle N,s|N^*\rangle_L|^2\,\delta(E_*(l,N)-E(l,N,s)-\varepsilon) \tag{15}$$

from a passive channel L. In the MND model the initial hole state $|N^*\rangle_L$ is made up of the N lowest orbitals (ψ_ν) of the core-hole Hamiltonian H^*_L. Similarly, all final states $|N,s\rangle_L$ can be taken as Slater determinants involving N orbitals (ϕ_ν) of the no-hole Hamiltonian H_L.

Keeping N finite, the required overlaps can be done numerically and, as has been shown in detail by previous workers,[10] they can all be expressed in the inverse of the $N\times N$ overlap matrix

$$S_{ij}=\langle\phi_i|\psi_j\rangle \tag{16}$$

involving the N lowest orbitals of H_L and H_L^*. For instance, the overlap $\langle N,s|N^*\rangle$ with a final state having a particle (μ) above and a hole (i) below the Fermi level is given by $\det(S)\sum_k\langle\phi_\mu|\psi_k\rangle S_{ki}^{-1}$. The energy of this final state is simply $\varepsilon_{l\mu}-\varepsilon_{li}+E(l,N)$, where $E(l,N)$ is the N-electron ground-state energy and $\varepsilon_{l\nu}$ is a one-electron eigenvalue of the no-hole Hamiltonian H_L. Multipair excitations can be handled in an analogous way, but it is generally found that one only needs to include up to double-pair excitations to satisfactorily exhaust the sum rule

$$\int A_l(\varepsilon)d\varepsilon=\sum_s|\langle N,s|N^*\rangle_L|^2=1$$

for N approximately 100.

An active channel involving the annihilation of a valence electron with the operator

$$c_M=\sum_k M_k c_{Lk} \tag{17}$$

can be handled by a similar method.[10,14] (The electron operators $\{c_{L\nu}\}$ refer to the no-hole Hamiltonian, and M_ν is a matrix element for the one-electron process in question.) The spectral profile is now

$$B_l(\varepsilon)=\sum_s|\langle N-1,s|c_M|N^*\rangle_L|^2\times\delta(E_*(l,N)-E(l,N-1,s)-\varepsilon)\ . \tag{18}$$

Using the expansion theorem for determinants, one can show[10] that the required overlaps $\langle N-1,s|c_M|N^*\rangle$ can be obtained by the same procedure as above applied to the overlap matrix

$$\begin{bmatrix}\langle\phi_1|\psi_1\rangle & \cdots & \langle\phi_1|\psi_N\rangle\\ \vdots & & \vdots\\ \langle\phi_{N-1}|\psi_1\rangle & \cdots & \langle\phi_{N-1}|\psi_N\rangle\\ \langle\chi_M|\psi_1\rangle & \cdots & \langle\chi_M|\psi_N\rangle\end{bmatrix},$$

where $\chi_M=\sum_k M_k\phi_k$.

In principle, we encounter in the Auger problem ($lm\sigma$) channels where two electrons are annihilated. Our LMTO calculations show, however, that these intrachannel parts are several orders of magnitude smaller than the remaining interchannel parts, and they can thus safely be neglected.

D. Choice of model parameters

In each L subchannel we represent the actual system by a model system with N fermions in a Hilbert space with N_0 levels. We model the local density of states (DOS) using a local orbital

$$c_L=\frac{1}{N_0}\sum_k u_l(\varepsilon_{lk})c_{Lk}\ , \tag{19}$$

where the energy levels and electron operator refer to the no-hole Hamiltonian H_L. In the ground state we identify the central-cell local DOS for the subchannel in question with the quantity

$$D_l(\varepsilon)=(2l+1)\sum_s|\langle N-1,s|c_L|N\rangle_L|^2\times\delta(E(N)-\varepsilon-E(N-1,s)) \tag{20}$$

and the number of l electrons in the central cell with n_l, where

$$n_l=\int_{-\infty}^{\mu}D_l(\varepsilon)d\varepsilon\ . \tag{21}$$

We then choose the occupied part of u_l such that D_l and n_l agree with our corresponding LMTO ground-state results in the bulk.

We next turn to the question how to represent the core-hole potential in the Hamiltonian

$$H_L^*=H_L+\frac{1}{N_0}\sum_{k,k'}V_{kk'}^l c_{Lk}^\dagger c_{Lk'}\ . \tag{22}$$

We take $V_{kk'}^l$ as a separable potential,

$$V_{kk'}^l=V_l u_l(\varepsilon_{lk})u_l(\varepsilon_{lk'})\ , \tag{23}$$

and choose V_l and the unoccupied part of the local state density so as to have (i) the Fermi-surface phase shift δ_l equal to a prescribed value, and (ii) the number of l electrons in the central cell,

$$n_l^*=\int_{-\infty}^{\mu}D_l^*(\varepsilon)d\varepsilon\ , \tag{24}$$

equal to the number of l electrons in the central cell with a core hole present according to our LMTO results. Here

$$D_l^*(\varepsilon)=(2l+1)\sum_s|\langle N-1^*,s|c_L|N^*\rangle_L|^2\times\delta(E(l,N^*)-\varepsilon-E(l,N-1^*,s)) \tag{25}$$

gives the model simulation of the local DOS in the presence of a static core-hole. It has been convincingly demonstrated[10] that the resulting dynamical spectra are almost independent of the functional form of the core-hole potential as long as the above constraints are satisfied. The form of the global state density D_0, which determines the separation of energy levels of a given channel, is also of little consequence for the dynamical results. We have here chosen D_0 as a semielliptic DOS containing N_0 levels, with N_0 approximately 200.

In order to model the matrix elements we assume that the Auger process can be satisfactorily described by a transition operator T which annihilates two electrons out of the relaxed ground state, i.e.,

$$T=\sum_{\nu,\nu'}T_{\nu\nu'}c_\nu c_{\nu'}\ . \tag{26}$$

With no loss of generality we can assume $T_{\nu\nu'}$ to be antisymmetric in the one-electron labels ν and ν'. As mentioned above, the intrachannel part of the Auger current

is completely negligible, and thus we can assume that ν and ν' refer to different $lm\sigma$ channels. In order to show that the Auger spectrum can be expressed in convolutions of zero- and one-electron spectral densities, we decompose the spectra in parallel (p) and antiparallel (a) spin components. We make a corresponding decomposition of $T_{\nu\nu'}$,

$$T_{\nu\nu'}=\tfrac{1}{2}T_{p,a}(\alpha,\alpha')(\delta_{\sigma\uparrow}\delta_{\sigma'\downarrow}\pm\delta_{\sigma\downarrow}\delta_{\sigma'\uparrow}) ,$$

where we model the antisymmetric and symmetric functions T_p and T_a by simple separable functions of the orbital labels α and α'. The d-electron contribution to the spectra is small and will not be considered. For the remaining contributions we take

$$T_{p,a}(\alpha,\alpha')=[(2l+1)(2l'+1)]^{-1/2} \times A_{ll'}^{p,a}u_l(\varepsilon_{lk})M_l(\varepsilon_{lk})u_{l'}(\varepsilon_{l'k'})M_{l'}(\varepsilon_{l'k'}) ,$$

except for the parallel-spin part for the case $l=l'=1$ where a somewhat more complicated ansatz is needed in order to obtain the required symmetry:

$$T_p(1mk,1m'k')=A_{11}^p\sum_{m,m'}\langle 10|1m,1m'\rangle u_1(\varepsilon_{1k}) \times M_1(\varepsilon_{1k})u_1(\varepsilon_{1k'})M_1(\varepsilon_{1k'}) .$$

(Here $\langle 10|1m,1m'\rangle$ is a Clebsch-Gordan coefficient.)

To determine the matrix element parameters A and M above, we require the model to correctly reproduce the LMTO ground-state results in the bulk when the core-hole effects are left out. An easy calculation shows that the model in this case gives the decomposed Auger spectrum

$$D_{ll'}^{p,a}(\varepsilon_A)=2\pi\int_{-\infty}^{\mu}d\varepsilon\int_{-\infty}^{\mu}d\varepsilon' D_l(\varepsilon)D_{l'}(\varepsilon')(A_{ll'}^{p,a})^2 \times M_l^2(\varepsilon)M_{l'}^2(\varepsilon')\delta(\varepsilon+\varepsilon'-\varepsilon_A) ,$$

and thus we determine the model parameters by fitting the properly symmetrized effective matrix element

$$\tfrac{1}{2}(A_{ll'}^{p,a})^2[M_l^2(\varepsilon)M_{l'}^2(\varepsilon')+M_l^2(\varepsilon')M_{l'}^2(\varepsilon)]$$

to the corresponding quantity obtained from the LMTO calculation [cf. I, Eqs. (24)–(26)]. The LMTO matrix elements are slowly varying functions of ε and ε' and are quite easy to fit.

With these prescriptions the calculation of a dynamical spectrum reduces to calculating recoil spectra $[A_l(\varepsilon)]$ and one-electron emission spectra $[B_l(\varepsilon)]$ by the finite-N method in each channel separately as described in the preceding subsection. The complete decomposed spectrum is then formed by convoluting together all eight channels. This step we do in time space. Thus, e.g., the time-space representation of the sp contribution is

$$D_{sp}(t)=[(A_{sp}^a)^2+(A_{sp}^p)^2]A_s(t)A_p^5(t)B_s(t)B_p(t) .$$

To do the Fourier transformation to time space we fit the finite-N result with a smooth function times the appropriate singularity factor, and transform the fit by a Gaussian integration procedure due to von Barth[34] which treats the singular part exactly. When transforming back the complete spectrum to energy space we apply a small Gaussian broadening $\exp(-\Delta^2t^2)$. We finally adjust the constants $A_{ll'}^{a,p}$ so as to exactly reproduce the correct subchannel yields $\Gamma_{ll'}^*$.

As a check of our procedure we performed MND calculations with zero potential and recovered the ground-state LMTO results with good accuracy.

IV. RESULTS

A. One-electron spectra from bulk atoms

We have obtained our Auger spectra in the bulk according to the theory given in I [cf. I, Eqs. (24)–(26)] and from self-consistent orbitals in the no-hole ground state. As we described in I, two different ways of approximating the final Auger orbitals have been used, namely (a) matching a proper solution inside the cell to free waves outside, and (b) approximating the Auger orbital by one single LAPW. As a measure of the error we are making in the different approximations we may, as discussed in I, Sec. III B, in the first method, (a) use the violation of the norm inside the central cell of the equivalent scattering state built of the spherical waves in question, and in the second method, (b) use the norm of that part ($\dot{P}$) of the wave function which is not a proper solution inside the cell. Now for the $L_{2,3}$ spectra we showed that the error involved when using the LAPW method was small for those partial waves which give important contributions to the Auger current, and we also showed that the spherical-wave method gives a rather small ($\sim 15\%$) violation of the norm condition. Thus we expect both methods to work well in these cases, and we also find that they give almost identical line shapes. This gives us some confidence in using the spherical-wave approximation for the K spectra, where the norm violation is still of the same order but where the error involved in the single LAPW approximation is larger. This is further supported by a recent calculation by Müller and Wilkins,[35] who find that the PDOS from the simple spherical-wave method is in quite reasonable agreement with suitably broadened full LAPW results at energies of the order 50–100 eV. Thus we use the first approximation (a) for the case of Li, Be, and Mg KVV spectra.

Our one-electron results are given and compared with experiment in Fig. 1 and decomposed into contributions from valence states of different angular momenta and spin in Fig. 2. We see that our pure one-electron results differ markedly from experiment and peak at too low energies. The different partial-wave contributions (ss,sp,pp) peak at rather different energies, and consequently the results are rather sensitive to errors in the matrix elements. It is thus appropriate to discuss whether the differences could be an artifact of our numerical methods used for the valence states. We believe this not the case. The LMTO method has been rather successfully applied to almost all kinds of solids (for reviews, see Ref. 8). In all cases investigated the main source of error has been the local approximation to exchange and correlation, not the LMTO method. In this work we have, in addition, improved the accuracy of the orbitals as discussed in I, Sec.

V. Further, approximations similar to ours have been used for calculating *KLV* spectra of Na,[11] and have been found to be in good agreement with experimental data.[39,40] The different partial-wave contributions peak at different energies also for *KLV* spectra, but their theoretical description is much simpler. In a *KLV* process there is a core vacancy also in the final state, and consequently there are no *dynamic* core-hole effects in this case. Furthermore, the surface is not expected to play a major role, due to the longer mean free path. We have used our relaxed impurity orbitals to calculate the *KLV* spectra also for Mg and Al (Ref. 41) and have obtained a rather similar agreement with experiment. There are no reasons why our approximations should give larger errors for *CVV* spectra. In view of this we believe that the differences between our one-electron bulk results and experiment are inherent to the one-electron and bulk approximations.

Unfortunately, our one-electron results do not agree as well with those by Jennison and co-workers.[2–4] For the case of Mg these workers[4] employ partly semiempirical matrix elements, but their results for Li and Be from

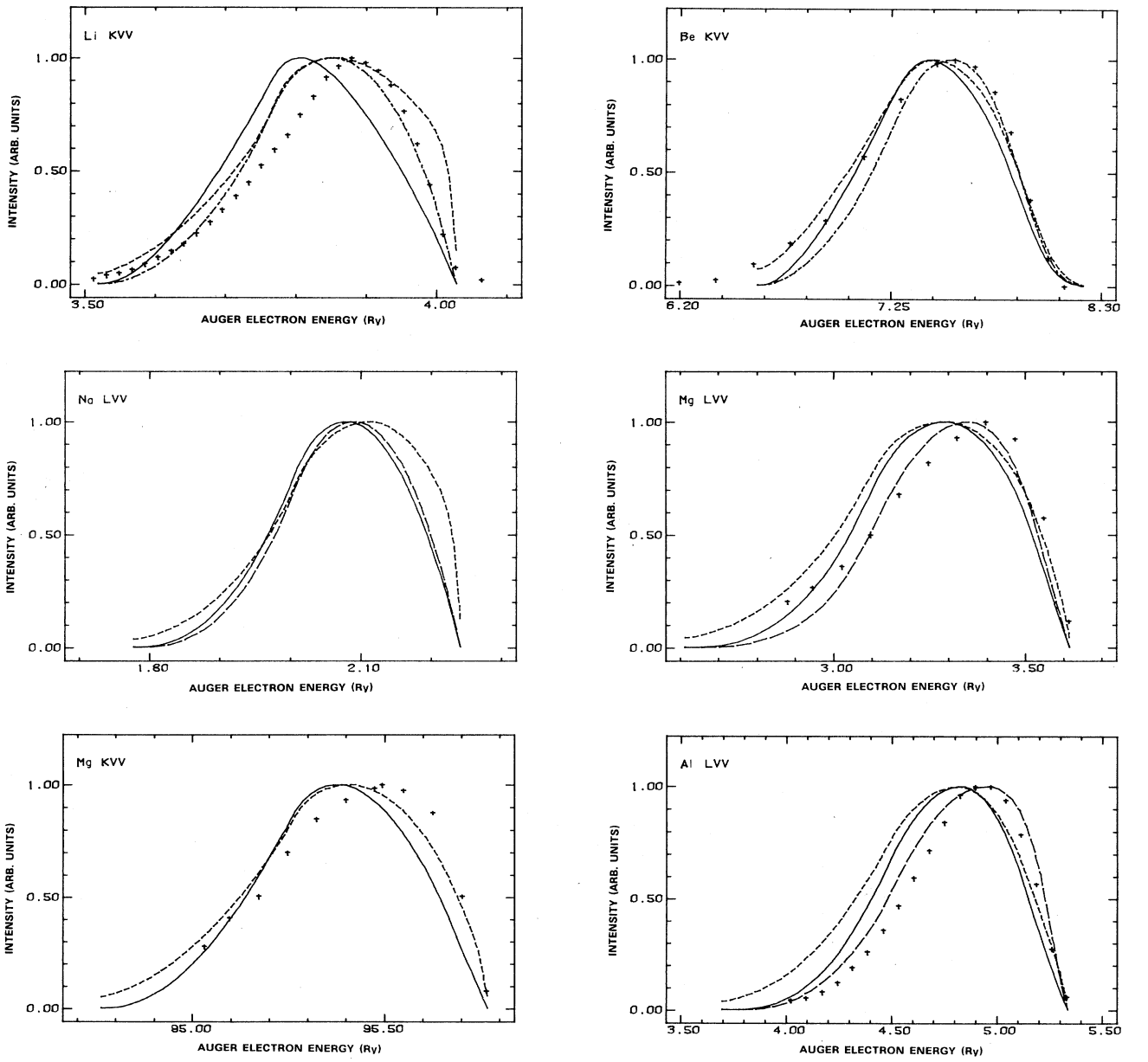

FIG. 1. Theoretical Auger line shapes compared with experiment. Solid curve, one-electron bulk theory; dashed-dotted curve, final-state rule, Eq. (12); short-dashed curve, full MND results; long-dashed curve, surface results from slab (Al) and IBM calculations. Experimental results (crosses) are taken from the following sources: Li, Ref. 36; Be, Ref. 3; Mg $L_{2,3}$, Ref. 37; Mg *K*, Ref. 4; Al, Ref. 38.

ground-state orbitals should be directly comparable to ours, but peak at higher Auger-electron energies. Jennison *et al.* use linear combinations of *s* and *p* Slater-type orbitals, which could possibly be argued to give a greater variational degree of freedom in the outer part of the Wigner-Seitz cell, but in the case of Be they do not carry their calculation to self-consistency. However, according to our experience the resulting spectra are not too sensitive to finer details in the valence-electron structure. For instance, we shall see in the following that IBM and slab calculations give almost indistinguishable spectra for an Al(100) surface despite noticeable differences in the density of states near the surface. We think instead that their different treatment of the Auger orbital might explain the differences. In I we argue that these orbitals, to a first approximation, should be solved in the same fully screened potential as is used for the other electrons. We have also solved the Auger orbitals in the fully screened hole potential of the initial state and obtained only minor differences, but Jennison *et al.* use a model with a Coulombic potential corresponding to a doubly charged ion in free space. The Coulombic tail may change the central-cell amplitudes of the different *l* components of the Auger-electron orbitals compared to the solutions ob-

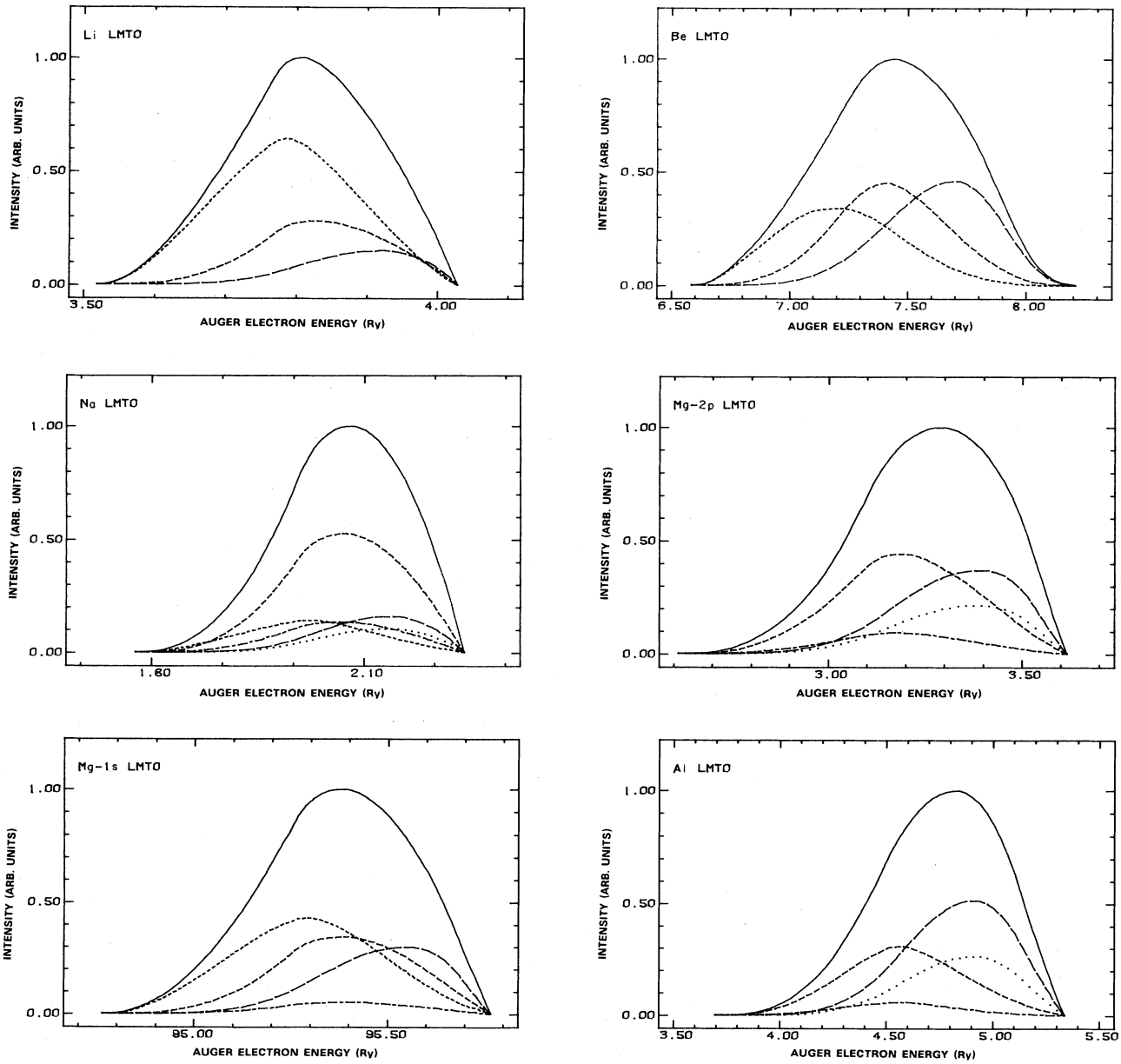

FIG. 2. One-electron Auger spectra in the bulk decomposed according to angular momentum and spin. Parallel and antiparallel spins of the final valence holes are denoted by *p* and *a*, respectively. Solid line, total spectrum; short-dashed lines, *ss* (*a*); medium-dashed lines, *sp* (*a*); dashed-dotted lines, *sp* (*p*); long-dashed lines, *pp* (*a*); dotted lines, *pp* (*p*).

tained from a screened potential. This in turn leads to different weights $\Gamma_{ll'}$ of the valence-electron channels. Which model is actually the most appropriate one has, at the present stage, to be judged *a posteriori* when corrections from the surface and from the core hole have been added to the one-electron bulk results.

B. Core-hole effects

According to the final-state rule, Eq. (12), the proper subchannel weights are those obtained with a static core hole. As is seen in paper I, Table IV, however, the relative weights $\Gamma_{ll'}/\Gamma$ for the third-row elements are almost unchanged when the orbitals are allowed to relax in the core-hole potential. Thus, this approximation does not improve the agreement with experiment in these cases. For the second-row metals, on the other hand, we see that the relative weights of the *sp* and *pp* channels increase when the effect of the core hole is introduced, which leads to a peak shift to higher energy and a much improved agreement with experiment (Fig. 1). For the case of Li, however, the peak still falls slightly below the correct position. We notice that the screening charge in Be has mainly *p* character (see paper I, Table III), whereas Jennison *et al.*[3] on the basis of a semiempirical theory argue that the core-hole screening mainly involves *s* electrons and that the screening leads to a peak shift to *lower* energies.

The weakness of static core-hole screening effect for the third-row metals may seem surprising in view of the rather strong effects seen in the corresponding *KLV* spectra.[39,40] These spectra have an anomalous shape, first explained by von Barth and Grossmann,[42] and show a pronounced distortion of the *s* DOS near the core hole. Because of the large *s*-wave distortion it has sometimes been assumed that core holes in these materials are screened mainly by *s* electrons. However, we here obtain *p*-wave screening charges which are comparable or larger than the *s*-wave parts, as did von Barth and Grossmann.[11] The orbitals nevertheless describe the *KLV* spectra and the *s* DOS distortion rather well.

We now turn to our fully dynamical calculations. Among the model parameters the ground-state transition densities of states, the local occupancies with and without a core hole, and the subchannel yields with a core hole present are uniquely determined by our LMTO calculations (cf. paper I, Tables III and IV). In addition, we also need estimates of the Fermi-surface phase shifts of the hole potential. Experimental and theoretical estimates span a wide range, particularly for Li and Na.[43] Our values (Table I) represent a compromise, and they are rather close to those obtained by Almbladh and von Barth,[44] except for Na, where we choose a smaller *s*-wave phase shift. Our phase shifts are also rather close to those which correspond to our core-hole screening charges. The values for Be are to be regarded as semiempirical and are chosen to be compatible with the observed small x-ray-photoemission-spectroscopy (XPS) asymmetry. In Be the strong band-structure effects and the noncubic symmetry almost certainly lead to modifications of both the Friedel sum rule[45] and the MND exponents.[46]

Our results are shown in Fig. 1, and decomposed spectra for Li and Na are shown in Fig. 3. In both Na and Li the peak moves to higher energies, and for Li the leading edge is actually too steep (Fig. 1). For lower energies our Li spectrum is broader than the experimental one. It must be remembered, however, that the experimental data are processed in such a way that the very intense plasmon satellite just below the maximum has been deconvoluted away. Looking at unprocessed data by Jackson *et al.*[47] it seems clear that reliable experimental information on an underlying no-loss spectrum is quite difficult to obtain below the leading edge. In addition, a deconvolution takes away the particle-hole shakeup losses which, in fact, are included in our dynamical spectra.

In the case of Na there are no undifferentiated spectra available in such a form that they readily allow detailed comparison. For the *KVV* spectrum of Mg the dynamical effects improve the agreement with experiment, although the leading edge is not steep enough (Fig. 1). For the remaining cases the MND calculations mainly give an overall broadening, due to particle shakeup, without changing the peak position. Thus we see (Fig. 1) that the bulk results for Mg $L_{2,3}$ and Al differ considerably from experiment also when dynamical core-hole effects are included. A possible explanation of the remaining discrepancy could possibly be that the hole-hole interactions left out in the MND model play an important role, but in general it has been found that hole-hole interactions tend to shift the intensity to *lower* energies.[18]

The effects of the core hole enter in two fundamentally different ways in Auger *CVV* spectra. They may redistribute the relative intensities among the subchannels, and they may cause a change in shape of individual subchannel spectra. As regards the initial-state rule for subchannel yields, it really does not rely on the MND model. Further, our impurity calculations should give quite reliable predictions of the relative weights $(\Gamma^*_{ll'}/\Gamma_*)$ and thus of the first effect. The second effect, on the other hand, relies in our calculations directly on a specific model. When the weights and screening charges are kept fixed, a dynamical MND spectrum depends essentially only on the Fermi-surface phase shifts (δ_l) of the core-hole potential. As mentioned above these phase shifts are not accurately known even for simple metals. For the case of Li one encounters difficulties when trying to reconcile the XPS exponent with results of inelastic electron scattering which show no trace of *s*-wave enhance-

TABLE I. Phase shifts used in the MND calculations.

	Li	Be	Na	Mg 1*s*	Mg 2*p*	Al
δ_s	0.620	0.032	0.719	0.460	0.458	0.398
δ_p	0.312	0.106	0.292	0.375	0.369	0.384

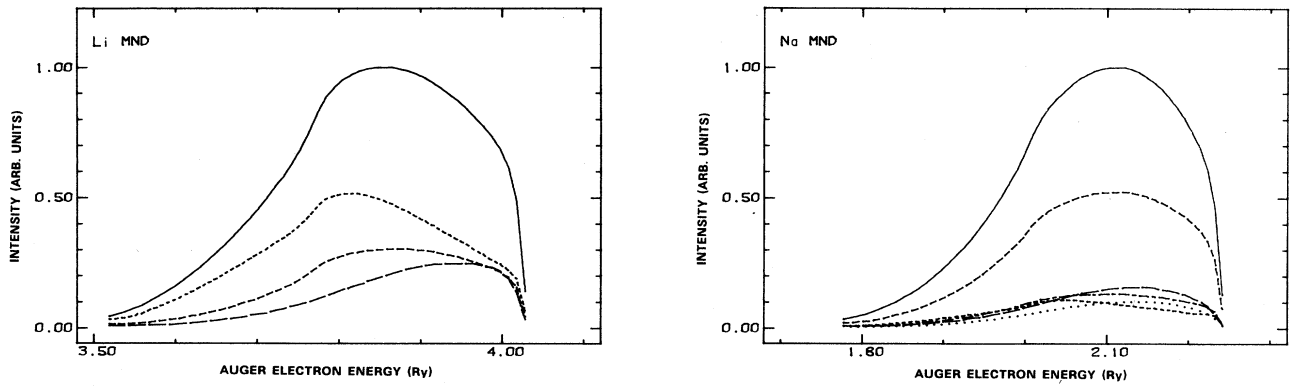

FIG. 3. Dynamical MND Auger spectra for Li and Na decomposed in subchannels as in Fig. 2.

ment (Sec. III A). Our calculations suggest that the MND model overestimates the dynamical effects also for the Li Auger spectrum. Calculations with a second set of phase shifts ($\delta_s=0.498$, $\delta_p=0.351$) gave rather similar results (Fig. 4), which supports the view that the problem with too strong dynamical effects in Li is inherent to the MND model itself.

As far as Na is concerned, both x-ray-emission and -absorption spectra no doubt show strong singularity effects, although they may be difficult to fit with a common set of phase shifts as required by the MND model. To test the sensitivity of the spectrum with regard to the parameters we have also for Na performed calculations with an alternative set of phase shifts ($\delta_s=0.43$, $\delta_p=0.38$). The change in the resulting dynamical spectrum is, however, hardly visible on the scale of Fig. 3. We believe the dynamical effects predicted by our MND calculations to be genuine, although their exact size may not be the correct one. We note that there are no significant redistributions among subchannels in the case of Na and that the entire effect is truly dynamical.

Dynamical calculations of core-hole effects have been presented earlier by Schulman and Dow.[5] Their results for the change in shape of subchannel spectra is in qualitative agreement with ours. However, since Schulman and Dow did not have access to spectra computed with impurity wave functions they were unable to predict the effect of intensity redistributions among the subchannels.

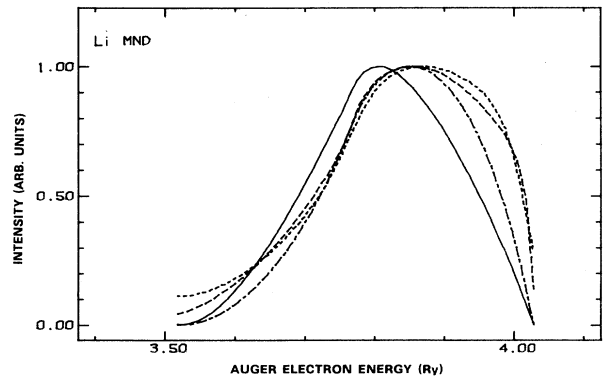

FIG. 4. Dynamical MND Auger spectra for Li corresponding to different sets of phase shifts. Medium-dashed curve, $\delta_s=0.620$, $\delta_p=0.312$; short-dashed curve, $\delta_s=0.498$, $\delta_p=0.351$. The one-electron (solid) and final-state rule (dashed-dotted) results are shown for comparison.

C. Surface effects

We now finally turn to the surface effects. Our calculations model (100) surfaces for the cubic metals and a surface perpendicular to the c axis for the hcp metals. In Fig. 5 we show the projected state densities for the first two layers and the bulk from our slab and IBM calculations. The number of s and p electrons in the different layers are given in Table II. We notice that the state densities from the IBM are not very far from those obtained from the slab calculation, but the number of p electrons in the first layer is somewhat overestimated. The resulting Auger spectra, however, are closer and, in fact, almost indistinguishable from each other. In view of this very good agreement it is reasonable to assume that the IBM does not introduce any serious errors for the other systems considered here. We see in Fig. 5 that only the first layer differs markedly from bulk behavior, the main effect being a transfer of DOS to higher energies. This effect is quite pronounced for Be, Mg, and Al. For Na, we obtain an intensity shift upwards for the s electrons but a shift to lower energies for the p electrons.

Our results for the Auger spectra at normal emission (Fig. 6) and for mean free paths given in Table III show a noticeable shift of the intensity maximum for the cases of Mg $I_{2,3}$ and Al as compared to the bulk case. For the monovalent metals Li and Na we have found that the surface gives no important effects despite changes in the local densities of states (cf. Fig. 1). For Mg and Al our (one-electron) results with the surface effects included agree quite well with experiment (see Fig. 1). For Al the MND effects only give a broadening, while for Mg we notice a small MND effect that would further improve the agreement. We have also computed spectra corresponding to an emission angle of 60° relative to the surface normal and found only minor changes of the line shapes.

The intrinsic intensity without the damping effects included gives, as discussed at length in I, a measure of the core-hole lifetime widths. In angle-resolved photoemis-

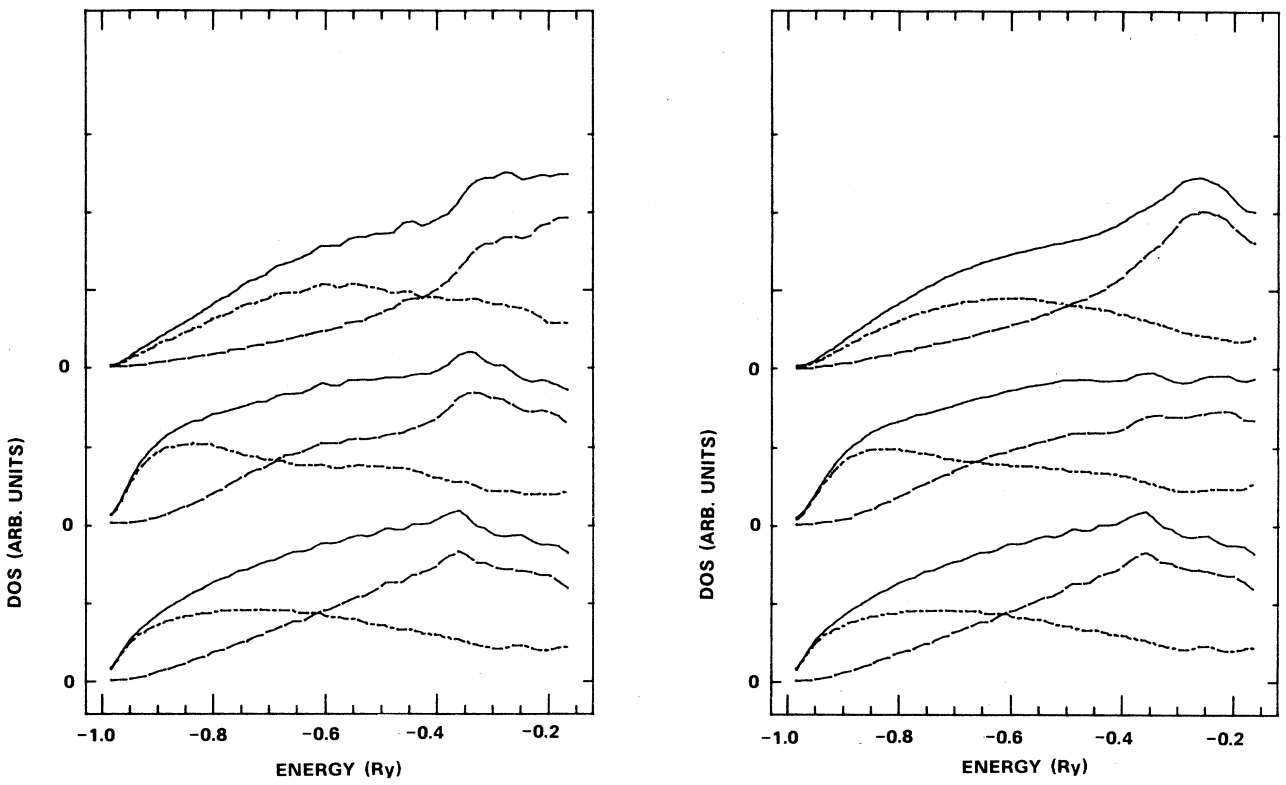

FIG. 5. Local density of states for the first two layers (top) and the bulk (bottom) for an ideal Al(100) surface according to slab (left-hand panel) and IBM (right-hand) calculations. The figure shows the local DOS (solid line) and its *s*-wave (dashed-dotted) and *p*-wave (long-dashed) components.

sion spectra a surface-enhanced core-level broadening has been observed[52] which sometimes has been attributed to a decreased core-hole lifetime. Our results here show no noticeable difference in intrinsic yields from bulk atoms and surface atoms, which seems to rule out this explanation.

All surface results were produced with the LAPW approximation for the Auger orbital. For the *K* spectra this approximation is not quantitative but probably good enough for obtaining general trends. Through comparison with the corresponding approximation in the bulk, we find that the surface effects are unimportant in the *K* spectra of Li, Be, and Mg.

V. CONCLUSIONS

In this paper we have presented one-electron calculations of Auger spectra in the bulk. We are quite convinced that these results are numerically accurate, but nevertheless they do not agree with experiment. To explain this discrepancy we have studied effects connected with the core hole in the initial state and effects connected with the surface and finite Auger-electron mean free path.

In the final-state approximation for core-hole-induced features one superimposes subchannel line shapes obtained with the final-state potential with weights obtained from the initial core-hole state. The reason for not

TABLE II. Number of electrons in the first three layers from the surface model (IBM) and from slab calculations.

		Li	Be	Na	Mg 2*p*	Al IBM	Al Slab
Layer 1	*s*	0.5	0.62	0.62	0.80	1.00	1.24
	p	0.36	1.24	0.27	0.89	1.34	1.20
Layer 2	*s*	0.5	0.63	0.61	0.91	1.12	1.13
	p	0.49	1.26	0.37	0.95	1.44	1.54
Layer 3	*s*	0.51	0.62	0.62	0.86	1.11	1.11
	p	0.46	1.26	0.35	0.94	1.46	1.46
Bulk	*s*	0.52	0.63	0.64	0.88	1.11	
	p	0.48	1.25	0.36	0.94	1.48	

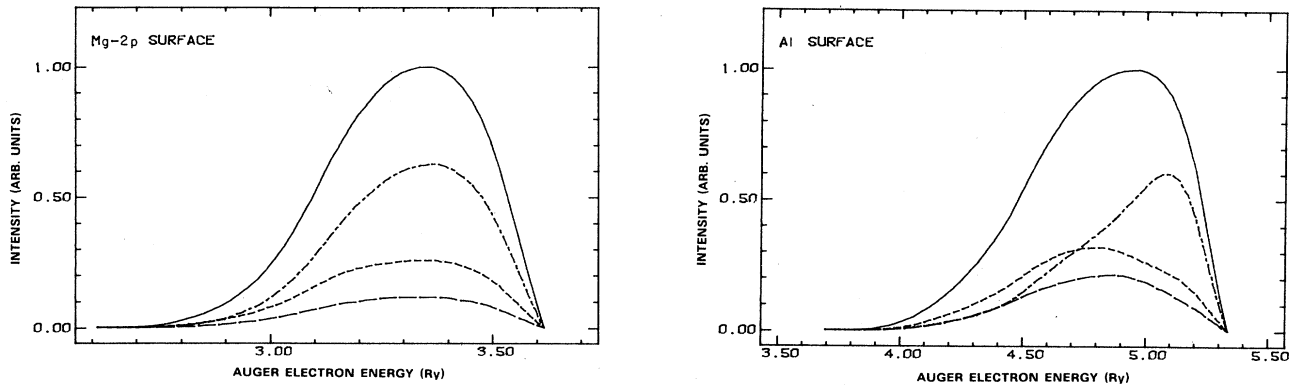

FIG. 6. Auger $L_{2,3}VV$ spectra from Mg and Al surfaces. The solid line gives the total spectrum, and the dashed-dotted, short-dashed, and long-dashed lines give the contributions from the first three layers, respectively.

changing the subchannel line shapes is partly based on empirical findings for x-ray spectra, and partly based on studies of the MND model. The reason for including core-hole screening in the weights is based on a model-independent sum rule. This approximation almost entirely removes the discrepancies between theory and experiment for the cases of Li and Be. The relative weights for the third-row metals, on the other hand, are almost unchanged upon introducing the core-hole effects, and thus the discrepancy here remains.

To study the dynamical effects on the partial line shapes we have performed fully dynamical calculations based on the MND model and with parameters chosen so as to reproduce our static self-consistent results as accurately as possible. For most cases we have found these dynamical effects to mainly produce an overall broadening due to particle-hole shakeup. For the monovalent metals Li and Na the partial contributions change in shape so as to move the intensity of the total spectrum to higher energies. We have also shown that the dynamical effects are insensitive to the precise values of the Fermi-surface phase shifts when all other model parameters (core-hole screening charges, etc.) are kept fixed. In the case of Li the dynamical part of the core-hole effects actually moves the theoretical curve away from experiment as compared to the final-state approximation. We have argued that we here encounter similar problems with the validity of the MND model as have been indicated by inelastic electron-scattering experiments. In the case of Na the MND collective effects are clearly present in soft-x-ray–emission (SXE) and soft-x-ray–absorption (SXA) spectra as well as in XPS spectra, although the consistency between the x-ray-emission and -absorption spectra may not be fully satisfactory. In view of this we believe that the dynamical peak shift we obtain for Na is a genuine effect, although its magnitude may be uncertain. However, there are no experiments available at present which allow for a detailed comparison.

We have obtained no evidence that the core-hole effects are important for the $L_{2,3}$ spectra of Mg and Al. In order to explain these spectra we have studied the effects of the surface and performed self-consistent slab calculations for an Al(100) surface. The slab spectra agree very well with the corresponding results from a much simpler infinite-barrier model, which we use for the remaining systems. Our spectra from Mg(100) and Al(100) surfaces agree very well with experiment. However, our treatment of the ejected Auger electron is still rather crude, and this close agreement may therefore be somewhat fortuitous. We nevertheless believe our results for the bulk and at the surface taken as a whole rather convincingly demonstrate the importance of surface effects in the $L_{2,3}VV$ spectra of Mg and Al. To map out these effects in a more accurate way, a full multiple-scattering treatment of the outgoing Auger electron would be required.

TABLE III. Mean free paths (Å) estimated from various experimental (Ref. 48) and theoretical sources (Refs. 49 and 50). The value 9 Å for Be is taken from Ref. 51.

Li	Be	Na	Mg 1*s*	Mg 2*p*	Al
4	9 5	3.5	17	3.5	4

ACKNOWLEDGMENTS

We are indebted to Ulf von Barth for generously sharing with us his experience in dynamical MND calculations. We also thank Günter Grossmann for useful discussions and collaboration in other parts of this project. One of us (A.L.M.) acknowledges financial support from the University of Antioquia and from the International Science Programs. The present work has also been supported in part by the Swedish Natural Science Research Council.

---

*Permanent address: Departamento de Física, Universidad de Antioquia, Apartado Areo 1226, Medellin, Colombia.

[1]P. J. Feibelman, E. J. McGuire, and K. C. Pandey, Phys. Rev. Lett. **36**, 1154 (1976); Phys. Rev. B **15**, 2202 (1977); P. J. Feibelman and E. J. McGuire, *ibid.* **17**, 690 (1978).

[2]D. R. Jennison, Phys. Rev. B **18**, 6865 (1978).

[3]D. R. Jennison, H. H. Madden, and D. M. Zehner, Phys. Rev. B **21**, 430 (1980).

[4]M. Davies, D. R. Jennison, and P. Weightman, Phys. Rev. B **29**, 5313 (1984).

[5]J. N. Schulman and J. D. Dow, Phys. Rev. Lett. **47**, 371 (1981); Int. J. Quantum Chem. Symp. **15**, 437 (1981).

[6]C.-O. Almbladh, A. L. Morales, and G. Grossmann, preceding paper, Phys. Rev. B **39**, 3489 (1989).

[7]O. K. Andersen, Phys. Rev. B **12**, 3060 (1975).

[8]O. K. Andersen, O. Jepsen, and D. Glötzel, in *Proceedings of the International School of Physics "Enrico Fermi," Course LXIX,* edited by F. Bassani, F. Fumi, and M. P. Tosi (North-Holland, Amsterdam, 1985); H. L. Skriver, *The LMTO Method* (Springer, Berlin, 1984).

[9]H. L. Skriver, Phys. Rev. B **31**, 1909 (1985).

[10]U. von Barth and G. Grossmann, Phys. Rev. B **25**, 5150 (1982).

[11]U. von Barth and G. Grossmann, Phys. Scr. **28**, 107 (1983).

[12]G. D. Mahan, Phys. Rev. **163**, 612 (1967); P. Nozières and C. T. De Dominicis, *ibid.* **178**, 1097 (1969).

[13]A. Kotani and Y. Toyozawa, J. Phys. Soc. Jpn. **35**, 1073 (1973); **35**, 1082 (1973); **37**, 912 (1974).

[14]C. A. Swarts, J. D. Dow, and C. P. Flynn, Phys. Rev. Lett. **43**, 158 (1980); J. D. Dow and C. P. Flynn, J. Phys. C **13**, 1341 (1980).

[15]L. C. Davis and L. A. Feldkamp, J. Appl. Phys. **50**, 1944 (1979); Phys. Rev. Lett. **44**, 673 (1980).

[16]D. E. Ramaker, Phys. Rev. B **25**, 7341 (1982).

[17]J. W. Gadzuk, Phys. Rev. B **9**, 1978 (1974).

[18]C. J. Powell, Phys. Rev. Lett. **30**, 1179 (1973); M. Cini, Solid State Commun. **20**, 605 (1976); G. A. Sawatzky, Phys. Rev. Lett. **39**, 504 (1977).

[19]C.-O. Almbladh, Nuovo Cimento B **23**, 75 (1974); Phys. Rev. B **16**, 4343 (1977).

[20]O. Gunnarsson and K. Schönhammer, Phys. Rev. B **22**, 3710 (1980).

[21]J. J. Chang and D. C. Langreth, Phys. Rev. B **5**, 3512 (1972).

[22]J. B. Pendry, in *Photoemission and the Electronic Properties of Surfaces,* edited by B. Feuerbacher, B. Fitton, and R. F. Willis (Wiley, New York, 1978), pp. 87–110. Recent discussions and further justifications have been given by C.-O. Almbladh [Phys. Scr. **32**, 341 (1985)] and by W. Bardyszewski and L. Hedin [Phys. Scr. **32**, 439 (1985)].

[23]P. Hohenberg and W. Kohn, Phys. Rev. **136**, B864 (1964); W. Kohn and L. J. Sham, *ibid.* **140**, A1133 (1965).

[24]E. U. Condon and G. H. Shortley, *The Theory of Atomic Spectra* (Cambridge University Press, London, 1970).

[25]Note that, in general, the spherical harmonics do not form an irreducible representation of the point group in question, and thus the muffin-tin coefficients B_L^k are not simply proportional to $Y_L^*(\hat{\mathbf{k}})$ as functions of $\hat{\mathbf{k}}$.

[26]J. D. Dow, Comments Solid State Phys. **6**, 71 (1975); J. Phys. F **5**, 1138 (1975).

[27]G. D. Mahan, Phys. Rev. B **11**, 4814 (1975).

[28]V. I. Grebennikov, Y. A. Babanov, and O. B. Sokolov, Phys. Status Solidi B **79**, 423 (1977); K. Schönhammer and O. Gunnarsson, Solid State Commun. **23**, 691 (1977).

[29]C.-O. Almbladh and L. Hedin, in *Handbook on Synchrotron Radiation,* edited by E. E. Koch (North-Holland, Amsterdam, 1983), Vol. 1b, pp. 607–904.

[30]J. J. Ritsko, S. E. Schnatterly, and P. C. Gibbons, Phys. Rev. B **10**, 5017 (1974).

[31]D. C. Langreth, Phys. Rev. B **1**, 471 (1970).

[32]R. V. Vedrinskii and J. Richter, Izv. Akad. Nauk. SSSR Ser. Fiz. **36**, 339 (1972) [Bull. Acad. Sci. USSR, Phys. Ser. **36**, 312 (1972)]; C.-O. Almbladh, Extended Abstracts of the Fourth International Conference on Vacuum-Ultraviolet Radiation Physics, Charlottesville, 1980 (unpublished).

[33]C.-O. Almbladh and U. von Barth, Extended Abstracts of the Fifth International Conference on Vacuum-Ultraviolet Radiation Physics, Monpellier, 1977 (a summary may be found in Ref. 29); T. T. Rantala, Phys. Rev. B **28**, 3182 (1983).

[34]U. von Barth (unpublished).

[35]J. E. Müller and J. W. Wilkins, Phys. Rev. B **29**, 4331 (1984).

[36]H. H. Madden and J. E. Houston, Solid State Commun. **21**, 1081 (1977).

[37]A. M. Baró and J. A. Tagle, J. Phys. F **8**, 563 (1978).

[38]J. E. Houston, J. Vac. Sci. Technol. **12**, 255 (1975).

[39]A. Barrie and F. J. Street, J. Electron Spectrosc. Relat. Phenom. **7**, 1 (1975).

[40]R. Lässer and J. C. Fuggle, Phys. Rev. **22**, 2637 (1980).

[41]C.-O. Almbladh and A. L. Morales (unpublished).

[42]U. von Barth and G. Grossmann, in Proceedings of the Eighth Annual Symposium on Electronic Structure of Metals and Alloys, Dresden, 1978, edited by P. Ziesche (Technische Universität, Dresden, 1978), p. 76.

[43]P. H. Citrin, G. K. Wertheim, and M. Schlüter, Phys. Rev. B **20**, 3067 (1979).

[44]C.-O. Almbladh and U. von Barth, Phys. Rev. B **13**, 3307 (1976).

[45]J. S. Langer and V. Ambegaokar, Phys. Rev. **121**, 1090 (1961).

[46]P. Lloyd, J. Phys. F **1**, 728 (1971); R. Schöpke, W. John, and E. Mrosan, J. Phys. F **9**, 1205 (1979).

[47]A. J. Jackson, C. Tate, T. E. Gallon, P. J. Bassett, and J. A. D. Matthew, J. Phys. F **5**, 363 (1975).

[48]D. A. Shirley, in *Photoemission in Solids I,* edited by M. Cardona and L. Ley (Springer, Berlin, 1978), pp. 165–193; H. Ibach, in *Electron Spectroscopy for Surface Analysis,* edited by H. Ibach (Springer, Berlin, 1977).

[49]C. J. Tung and R. H. Ritchie, Phys. Rev. B **16**, 4302 (1977).

[50]B. I. Lundqvist, Phys. Status Solidi **32**, 273 (1969).

[51]M. P. Seah, Surf. Sci. **32**, 703 (1972).

[52]W. Eberhardt, G. Kalkoffen, and C. Kunz, Solid State Commun. **32**, 901 (1979).